KeAi

CHINESE ROOTS
GLOBAL IMPACT

Contents lists available at ScienceDirect

#### Petroleum Science

journal homepage: www.keaipublishing.com/en/journals/petroleum-science



#### **Original Paper**

### Study on the effect of clay minerals on phase transition of methane hydrate in sand sediments: Kinetic behavior and microstructural observation



Xinxu Wang <sup>a, b, c</sup>, Yuan Yuan <sup>a, b</sup>, Zhongming Du <sup>a, b</sup>, Bo Liu <sup>c</sup>, Chenlu Xu <sup>d</sup>, Jijin Yang <sup>a, b, \*</sup>

- <sup>a</sup> Key Laboratory of Deep Petroleum Intelligent Exploration and Development, Institute of Geology and Geophysics, Chinese Academy of Sciences, Beijing, 100029, China
- <sup>b</sup> College of Earth and Planetary Sciences, University of Chinese Academy of Sciences, Beijing, 100049, China
- <sup>c</sup> State Key Laboratory of Continental Shale Oil, Northeast Petroleum University, Daqing, 163318, Heilongjiang, China
- <sup>d</sup> Guangzhou Marine Geological Survey, Ministry of Natural Resources, Guangzhou, 510075, Guangdong, China

#### ARTICLE INFO

# Article history: Received 15 November 2024 Received in revised form 26 February 2025 Accepted 31 March 2025 Available online 1 April 2025

Edited by Min Li

Keywords:
Methane hydrate
Clay minerals
Formation kinetics
Microstructure
Depressurization

#### ABSTRACT

Natural gas hydrates widely accumulate in submarine sediments composed of clay minerals. However, due to the complex physiochemistry and micron-sized particles of clay minerals, their effects on methane hydrate (MH) formation and dissociation are still in controversy. In this study, montmorillonite and illite were separately mixed with quartz sand to investigate their effects on MH formation and dissociation. The microstructure of synthesized samples was observed by cryo-SEM innovatively to understand the effects of montmorillonite and illite on MH phase transition in micron scale. Results show that montmorillonite and illite both show the inhibition on MH formation kinetics and water-tohydrate conversion, and illite shows a stronger inhibition. The 10 wt% montmorillonite addition significantly retards MH formation rate, and the 20 wt% montmorillonite has a less inhibition on the rate. The increase of illite mass ratio (0-20 wt%) retards the rate of MH formation. As the content of clay minerals increase, the water-to-hydrate conversion decreases. Cryo-SEM images presented that montmorillonite aggregates separate as individual clusters while illite particles pack as face-to-face configuration under the interaction with water. The surface-overlapped illite aggregates would make sediments pack tightly, hinder the contact between gas and water, and result in the more significant inhibition on MH formation kinetics. Under the depressurization method, the addition of clay minerals facilitates MH dissociation rate. Physicochemical properties of clay minerals and MH distribution in the pore space lead to the faster dissociation rate in clay-containing sediments. The results of this study would provide beneficial guides on geological investigations and optimizing strategies of natural gas production in marine hydratebearing sediments.

© 2025 The Authors. Publishing services by Elsevier B.V. on behalf of KeAi Communications Co. Ltd. This is an open access article under the CC BY-NC-ND license (http://creativecommons.org/licenses/by-nc-nd/4.0/).

#### 1. Introduction

Natural gas hydrates are nonstoichiometric crystalline solids composed of gas molecules trapped in lattices formed by water molecules (Sloan and Koh, 2007). They widely distribute in the global submarine and permafrost sediments and remain stable within certain high pressure and low temperature conditions

\* Corresponding author.

E-mail address: yang@mail.iggcas.ac.cn (J. Yang).

Peer review under the responsibility of China University of Petroleum (Beijing).

(Kvenvolden, 2002). Methane hydrate (MH) is the predominant type of naturally occurring gas hydrates (Boswell and Collett, 2011). The global estimate of carbon stored in natural gas hydrates is about 500–2300 gigatons (Piñero et al., 2013; Ruppel and Kessler, 2017), making them as a potential energy (Ruppel, 2007).

Marine sediments contain about 99% of the global natural gas hydrate accumulations and most natural gas hydrates occur in the fine-grain sediments (Boswell and Collett, 2006; Ruppel, 2015; Waite et al., 2009). In addition to quartz, clay minerals are the major composition of gas hydrate-bearing sediments (GHBS) in submarine (Li et al., 2019; Meazell et al., 2020). Clay-rich submarine sediments have low permeability, weak consolidation and higher

risk of seafloor subsidence occurrence (Liu et al., 2023; Moridis et al., 2013; Shaibu et al., 2021; Yang et al., 2018). The investigations of MH formation and dissociation in the claycontaining GHBS are essential for estimating energy storage, developing safe and economic strategies and protecting submarine infrastructures during natural gas hydrate exploitation (Canals et al., 2004; Constant Agnissan et al., 2024; Yin et al., 2016).

Montmorillonite (smectite) and illite are the dominant clay minerals in GHBS in Indian continental margin, the Blake Ridge and the South China Sea (Collett and Wendlandt, 2000; Phillips et al., 2014; Wang et al., 2022). Due to the various crystal structures and physicochemical properties, the roles of clay minerals on MH formation and dissociation are complex. Montmorillonite has been widely investigated and its effect on MH formation and dissociation is still controversial. Montmorillonite has been found to promote MH nucleation and formation due to its large surface area for providing more nucleation sites (Cha et al., 1988; Cygan et al., 2004; Park and Sposito, 2003) and its negative-charged surface for creating an electric field (Ren et al., 2022). The induction time of MH formation has been reported to decrease with montmorillonite content increase (10-25 wt%) in silica sands (Zeng et al., 2022). In addition, montmorillonite facilitates MH dissociation in claycontaining silts (Ma et al., 2022). However, other studies have also found that montmorillonite increases the induction time and retards the rate of MH growth and dissociation, resulting from reducing the porosity and decreasing the diffusion of methane gas and water (Kumar et al., 2015; Nair et al., 2018; Ren et al., 2022; Zhang et al., 2017).

Illite is another dominant clay mineral in marine GHBS. Few studies have analyzed the effect of illite on formation of MH and there is no consistent conclusion. Illite has been found to increase the rate of MH formation in sand at low content (10 wt%), but decrease MH formation rate as illite increases from 20 to 40 wt% (Chen et al., 2024). However, illite has been observed to inhibit MH formation kinetics in sediments with the lower illite content of 10 wt% and the induction time remains relatively constant at the higher illite content from 20 to 60 wt% (Constant Agnissan et al., 2024).

It is noted that most investigations about the effect of clay minerals on the kinetic behaviors of MH phase transition are analyzed mainly on the basis of the evolution of temperature and pressure during the experiments, which could not fully understand the effect of clay minerals. Visualization method has been applied to investigate the kinetics of MH formation and dissociation in presence of clay minerals. Nuclear Magnetic Resonance system was used to observe the water distribution to study MH formation and dissociation in porous media filled with montmorillonite/illite suspension, and found that clay minerals increase water conversion rate and retards MH initial dissociation rate (Feng et al., 2023). The high-resolution camera has been employed to observe MH layer and clay layer in different clay suspensions to analyze the factors of MH formation and dissociation kinetics (Ren et al., 2022, 2024). Nevertheless, clay minerals are the micron-sized particles and methane hydrate nucleation typically occurs at the nanometer scale (Guo and Zhang, 2021). Due to the limitation of resolution, it is still essential to apply higher-resolution imaging techniques to observe the effect of clay minerals on MH phase transition.

Cryogenic scanning electron microscopy (cryo-SEM) has shown great potential to investigate the microstructure of hydrate-bearing sediments from geological reservoir and artificially synthesized sample (e.g. Stern and Lorenson, 2014; Wang et al., 2024). With the advantage of high resolution in micron and sub-micron scale, the microstructure of hydrate-bearing sediments could be beneficial to analyze the effect of clay minerals on MH.

In this study, the kinetic behaviors of MH phase transition in

quartz sands with and without montmorillonite/illite were studied and the microstructure of the synthesized samples were investigated by cryo-SEM observation. This study innovatively applied cryo-SEM to directly observe the microstructural difference between the aggregates of montmorillonite and illite and the hydrate distribution in synthesized sediments, and explained the effects of clay minerals on kinetic behaviors of MH phase transition in micron scale. The experimental results of this study would provide insights for understanding the accumulation and exploration of natural gas hydrate in clay-containing marine sediments.

#### 2. Materials and methods

#### 2.1. Materials and experimental apparatus

In this study, methane gas (99.999% purity) and distilled water were used for MH synthesis. Quartz sands (Hunyuanjunhongxin Material Co. Ltd., China) range from 100 to 600  $\mu$ m and the grain size distribution shows in Fig. 1. Na-montmorillonite and illite were obtained from Shanlinshiyu Mineral Product Co. Ltd., China. Microstructure and EDS analysis of montmorillonite and illite are shown in Fig. 2.

MH formation and dissociation experiments were conducted in Core Labs, Institute of Geology and Geophysics, Chinese Academy of Sciences. Fig. 3 shows the schematic of experimental apparatus in this study. A high-pressure vessel made of nickel alloy GH132 is 6 cm in diameter with 17 cm in height and the maximum working pressure is up to 30 MPa. Water jacket coating the high-pressure vessel is used to control the temperature inner the vessel by a low temperature thermostat with an accuracy of  $\pm 0.1$  K and the lowest temperature could reach 253.2 K. Two Pt100 thermocouples (measurement accuracy  $\pm 0.1$  K) are placed in the distance of 8 cm and 4 cm respectively from the bottom of the vessel to measure the experimental temperature. A pressure transducer (measurement range 0–30 MPa) is connected with the top of the vessel to measure the experimental pressure with accuracy of 0.25% full scale (FS). A back-pressure valve set by a hand-in pump is used to control the outlet pressure of a mass flow controller (D07-11C, Beijing Sevenstar Flow Co., Ltd., accuracy of 1% FS) and regulates the flow rate of methane gas into the high-pressure vessel. A syringe pump (260 D, Teledyne Isco, USA) is connected with the outlet of the highpressure vessel and controls the rate of methane gas released from the vessel. A mass flowmeter (D07-7CM, Beijing Sevenstar Flow Co., Ltd., accuracy of 1.5% FS) is used to measure the amount of gas released from the vessel during hydrate dissociation experiments. The temperature and pressure data are collected by data collection system and were recorded every 15 s for all of the experiments in this study.

#### 2.2. Methane hydrate formation experiments

It is noted that clay mineral in sediments in the production test in Shenhu Area, the South China Sea is 26–31 wt% and the smectite content ranges from 4.7 to 18.6 wt% in sediments from the production test site at East Nankai Trough, Japan (Egawa et al., 2015; Li et al., 2018; Ren et al., 2024). Therefore, a clay content up to 20 wt% was chosen in this study.

Before all of the experiments, quartz, Na-montmorillonite and illite were respectively dried in the oven under 383.2 K for more than 12 h. To prepare the clay-containing sediments, Na-montmorillonite and illite were separately mixed with quartz sands. The water content, namely the mass ratio of water and sediments, is the same for all of the MH formation experiments. Sediments were mixed with distilled water uniformly, packed into the high-pressure vessel and compacted with a rob. After the vessel

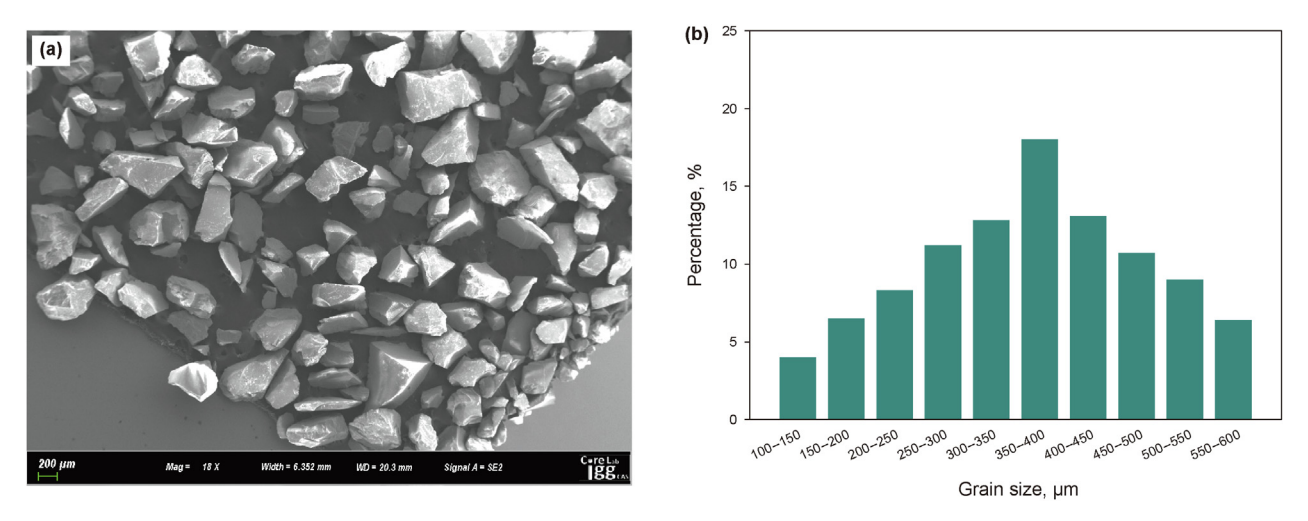


Fig. 1. SEM image (a) and grain size distribution (b) of quartz sands.

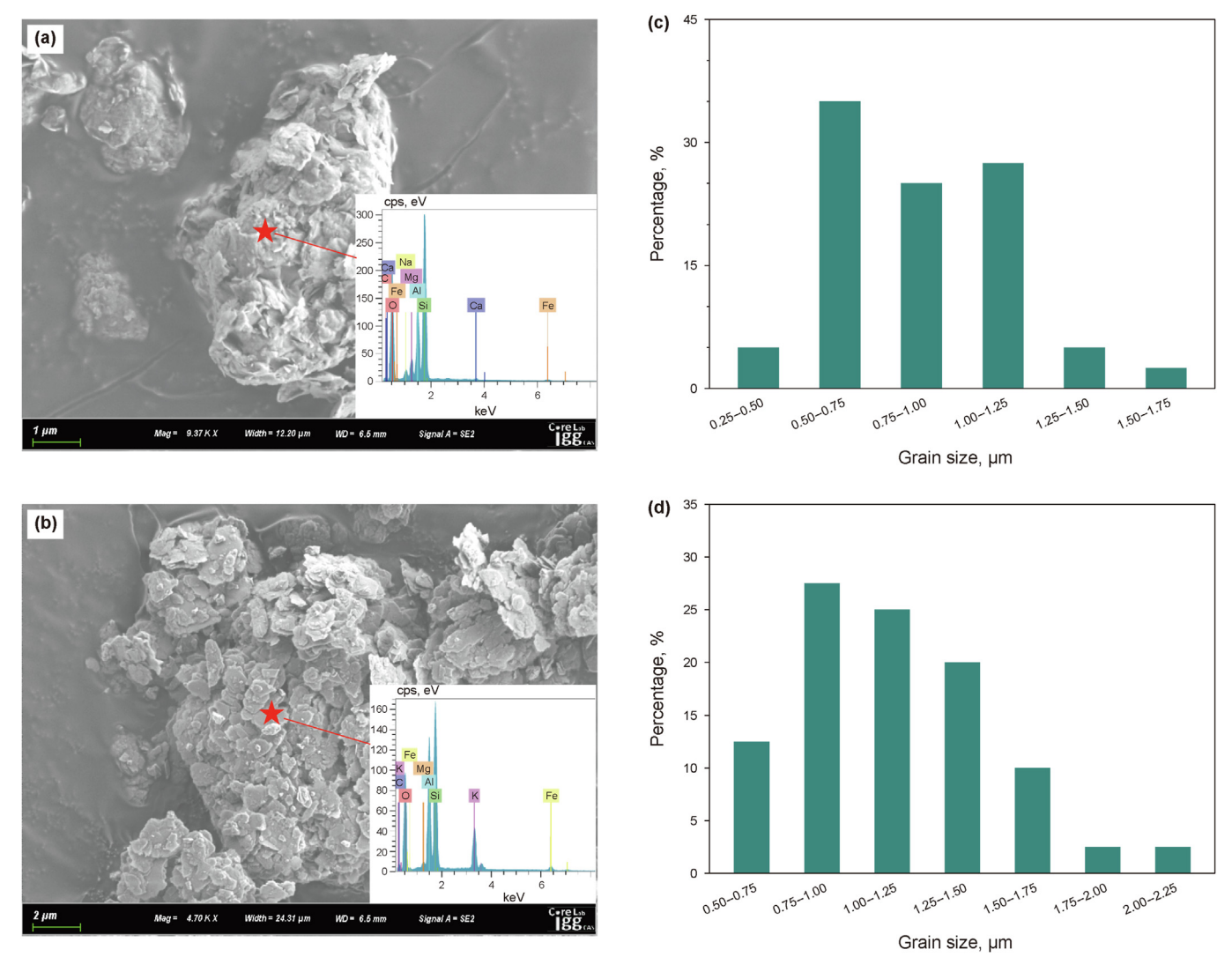


Fig. 2. SEM images and EDS analysis of montmorillonite (a) and illite (b) used for experiments. Grain size distributions of montmorillonite (c) and illite (d).

was sealed and vacuumed, methane gas was slowly injected into the vessel from the bottom to pressurize the vessel. All of the valves were closed until the pressure in the vessel was up to about 8 MPa. After the experimental pressure was stable, the high-pressure

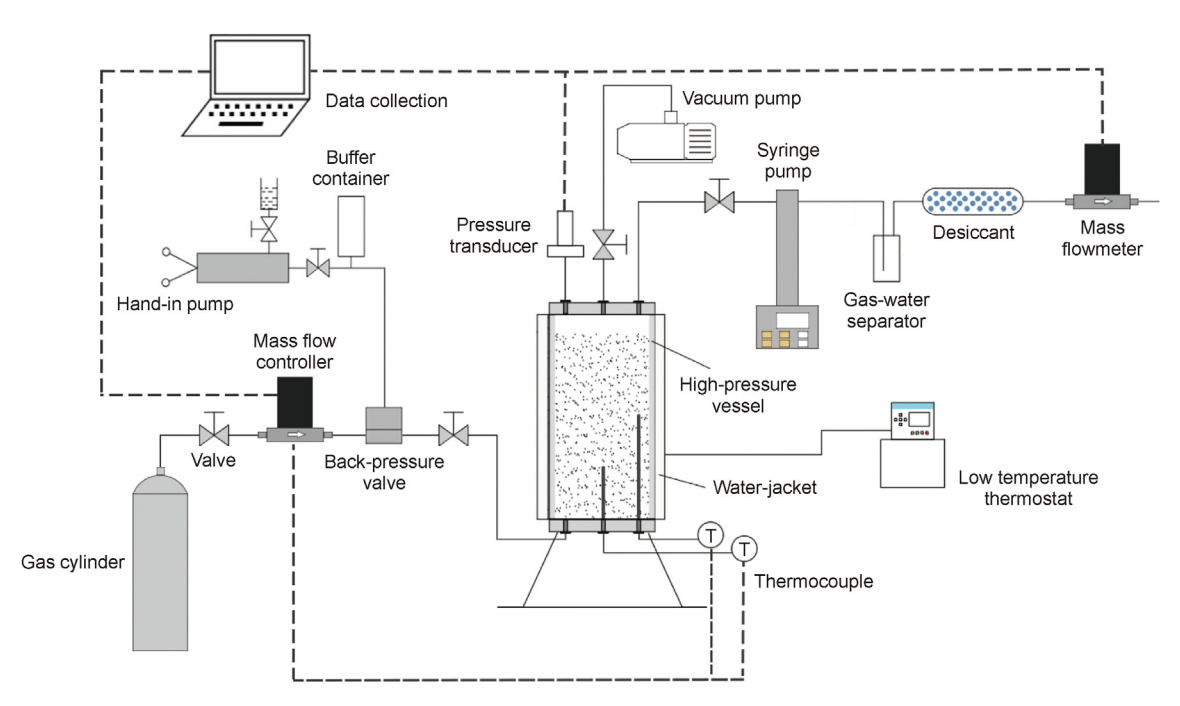


Fig. 3. The schematic diagram of the experimental apparatus.

vessel was then cooled to about 275.2 K. During the synthesis experiments, the appearance of thermal spike indicates the onset of MH growth. When the rate of pressure reduction was less than 0.02 MPa/h, the synthesis of MH could be considered as completion. The detail conditions of MH formation experiments are listed in Table 1.

#### 2.3. Cryo-SEM imaging observation

After MH formation experiments, the synthesized hydratebearing sediments in Experiments 3 and 5 were recovered from the high-pressure vessel quickly and stored in the liquid nitrogen. For the pure quartz sediments in Experiment 1, after MH synthesized and the pressure kept at the equilibrium pressure, 0.129 mol gas was injected into the vessel again to make more MH synthesized. The pure quartz sediments were then recovered and stored in the liquid nitrogen. Samples were trimmed and polished in the liquid nitrogen pool of the Baygon Cryo MCP 100 (Baygon Scientific (Suzhou) Co., Ltd., China). The detail preparation of cryo-SEM imaging refers to Wang et al. (2024). The microstructure of the sediments was imaged under cryo-SEM (Zeiss Merlin in Core Labs. Institute of Geology and Geophysics, Chinese Academy of Sciences). The accelerating voltage was 1–2 kV for microstructure imaging. Energy dispersive X-ray spectroscopy (EDS) with SEM was applied to analyze the material phase and the working accelerating voltage was 5 kV.

#### 2.4. Methane hydrate dissociation experiments

Before MH dissociation experiments started, MH was first synthesized in pure quartz sand with/without mixed with clay minerals. The sediment preparation is the same as that in Section 2.2 for MH formation experiments. After the vessel was sealed and vacuumed, the vessel was pressurized by injecting methane gas and kept at about 8 MPa to providing sufficient gas during the whole process of MH synthesis. The vessel was then cooled to 274.9 K to start MH formation. When the pressure and temperature of the vessel were stable and no more methane gas was injected into the vessel, MH synthesis was considered to be completed. The valves connected with the bottom of the vessel were closed to stop methane gas injection. To prevent ice formation and MH secondary formation, the rate of gas release was set as 15 mL/min at the standard temperature and pressure condition to start the hydrate dissociation experiments. Mass flowmeter was used to measure the amount of methane gas released from the vessel during the whole depressurization process. The detail conditions of MH dissociation experiments are listed in Table 2.

#### 2.5. Calculation

#### 2.5.1. Growth kinetics of methane hydrate

The calculations of MH formation rate and water-to-hydrate conversion can be referred to the pore-volume balance method in Chong et al. (2016) and Ren et al. (2023). The dissolution of

**Table 1** Experimental conditions of methane hydrate formation.

Exp.No.	Clay mineral		Quartz mass, g	Water mass, g	Water content, %	Porosity, %	Gas injection, mol	P <sub>Initial</sub> , MPa	P <sub>Final</sub> , MPa	T <sub>Initial</sub> , K	
	Type	Mass fraction, wt%	Mass, g								
Ex1	_	_	_	530	89.8	17	42.7	0.540	8.52	3.30	293.7
Ex2	MMT	10	46.7	420.1	77.5	17	43.2	0.652	8.24	4.78	294.8
Ex3	MMT	20	93.4	373.4	77.5	17	51.3	0.661	8.18	4.87	296.5
Ex4	III	10	46.7	420.1	77.5	17	41.9	0.634	8.09	5.15	294.4
Ex5	III	20	93.4	373.4	77.5	17	40.4	0.621	7.98	6.25	296.5

 Table 2

 Experimental conditions of methane hydrate dissociation.

Exp.	Clay mine	Clay mineral			Porosity, %	Water mass, g	Water content, %
No.	Туре	Mass fraction, wt%	Mass, g				
Ex6	_	_		460	42.1	92	20
Ex7	MMT	20	92	368	52.5	92	20
Ex8	III	20	92	368	41.4	92	20

methane gas in water is negligible due to the low solubility of methane gas (Poling et al., 2001; Sloan and Koh, 2007). During the formation of MH, the residual methane gas in the vessel at time *t* is described from gas law by Eq. (1).

$$n_{g,t} = \frac{P_t}{ZRT_t} \times V_{g,t} \tag{1}$$

where  $n_{g,t}$  is the mole number of free gas in the vessel,  $P_t$  is the pressure,  $V_{g,t}$  is the volume of the free gas in the vessel. Z is the compressibility factor at  $P_t$  and  $T_t$  condition by Pitzer's correlation (Smith et al., 2001), R is the universal gas constant (8.314 J/(mol·K)) and  $T_t$  is the average temperature from the two thermocouples set in the vessel.

During the formation experiment, the total volume of free gas, water and MH in the vessel ( $V_{\rm void}$ ) was constant. The volume of free gas, water and MH ( $V_{\rm g,t}$ ,  $V_{\rm w,t}$  and  $V_{\rm h,t}$ ) in the vessel at time t is given by:

$$V_{\text{void}} = V_{\text{g},t} + V_{\text{w},t} + V_{\text{h},t} = V_{\text{g},t} + \frac{(n_{\text{w},0} - \Delta n_{\text{w},t})M_{\text{w}}}{\rho_{\text{w}}} + \frac{\Delta n_{\text{h},t}M_{\text{h}}}{\rho_{\text{h}}}$$
(2)

where  $n_{\rm W,0}$  is the mole number of initial water before MH formation.  $\Delta n_{\rm W,t}$  and  $\Delta n_{\rm h,t}$  are the mole numbers of consumed water and synthesized MH at time t, respectively.  $M_{\rm W}$  and  $M_{\rm h}$  are the molar masses of water and MH, respectively.  $\rho_{\rm W}$  and  $\rho_{\rm h}$  are the densities of water and MH, respectively. The molar volumes of water and MH are 18 and 136.7 cm<sup>3</sup>/mol, respectively (Waite et al., 2009).

At time t, the consumption of methane gas and water and the synthesized MH can be described by Eqs. (3)–(5):

$$n_{g,t} = n_{g,0} - \Delta n_{g,t} \tag{3}$$

$$\Delta n_{g,t} = \Delta n_{h,t} = \frac{\Delta n_{w,t}}{N_w} \tag{4}$$

$$\Delta n_{\mathbf{W},t} = \mathsf{C}_t \times n_{\mathbf{W},0} \tag{5}$$

where  $n_{g,0}$  is the initial number of moles of methane gas in the vessel,  $\Delta n_{g,t}$  is the number of moles of free gas consumed to synthesize MH.  $N_{\rm W}$  is the hydration number which is assumed to be 6 (Sloan and Koh, 2007).  $C_t$  is the conversion of water to MH. Combining the above equations,  $C_t$  is the only unknown and can be calculated by meeting the  $P_t$  and  $T_t$  conditions at time t. The rate of MH formation is as follows:

$$\Delta N_{g,t} = \frac{\Delta n_{g,t}}{n_{w,0}} \tag{6}$$

$$r_{\rm g} = \frac{\Delta N_{\rm g, t_2} - \Delta N_{\rm g, t_1}}{t_2 - t_1} \tag{7}$$

where  $\Delta N_{g,f}$  is the normalized consumption of free gas (mol of gas/mol of water).  $r_g$  is the normalized rate of MH formation at the time

interval between  $t_2$  and  $t_1$ . The MH formation rate is calculated every 30 min.

#### 2.5.2. Methane hydrate dissociation kinetics

MH dissociation kinetics can be calculated using the method given by Chong et al. (2016, 2017). During the MH dissociation, the free gas in the vessel at time j is described by Eq. (8).

$$n_{g,j} = \frac{P_t}{ZRT_t} \times V_{g,j} \tag{8}$$

where  $n_{g,j}$  is the mole number of free gas and  $V_{g,j}$  is the volume of free gas in the vessel at time j.

The total volume of free gas, water and MH is constant during the experiment expressed by Eq. (9). During MH dissociation, the total number of moles of methane  $(n_{g,total})$  is the sum of mol number of free gas in the vessel  $(n_{g,j})$ , residual MH  $(n_{h,j})$  and the free gas released out of the vessel  $(n_{r,j})$  at time j. The number of moles of methane gas in the vessel is expressed by Eq. (10).

$$V_{\text{void}} = V_{g,j} + V_{w,j} + V_{h,j} = V_{g,j} + \frac{(n_{w,i} - \Delta n_{w,j})M_{w}}{\rho_{w}} + \frac{(n_{h,i} - \Delta n_{h,j})M_{h}}{\rho_{h}}$$
(9)

$$n_{g,total} = n_{g,j} + n_{h,j} + n_{r,j}$$
 (10)

where  $V_{\mathrm{g},j}$ ,  $V_{\mathrm{w},j}$  and  $V_{\mathrm{h},j}$  are the volume of free gas, water and MH in the vessel at time j, respectively.  $n_{\mathrm{w},i}$  and  $n_{\mathrm{h},i}$  are the mole numbers of initial water before MH formation and total synthesized MH before MH dissociation, respectively.  $\Delta n_{\mathrm{w},j}$  and  $\Delta n_{\mathrm{h},j}$  are the mole numbers of consumed water and decomposed MH at time j, respectively.

During MH dissociation, the mole numbers of MH and water changed can be described as follows:

$$\Delta n_{h,j} = n_{h,i} - n_{h,j} = n_{h,i} \times x_j \tag{11}$$

$$\Delta n_{w,j} = N_w \times \Delta n_{h,j} \tag{12}$$

where  $x_j$  is the fraction of decomposed MH at time j. Combining Eqs. (8)–(12),  $x_j$  is the only unknown and can be calculated by meeting the  $P_t$  and  $T_t$  conditions at the time j during MH dissociation. The normalized volume of methane gas production from MH dissociation between time  $j_2$  and  $j_1$  ( $m^3$  of gas/( $m^3$  of MH·h)) can be calculated by Eq. (13).

$$V_{g,n} = \frac{\Delta n_{h,j} \times 0.02271}{n_{h,i}/\rho_h \times (j_2 - j_1)}$$
 (13)

where the molar volume of methane gas is 0.002271 m<sup>3</sup>/mol at standard temperature and pressure (Chong et al., 2017).  $\rho_h$  here is the molar density of MH (7460 mol/m<sup>3</sup>) according to MH density of 925 kg/m<sup>3</sup> (Waite et al., 2009) and hydration number of 6. The

average volume of normalized methane gas production form dissociated hydrate is calculated every 30 min.

#### 3. Results and discussion

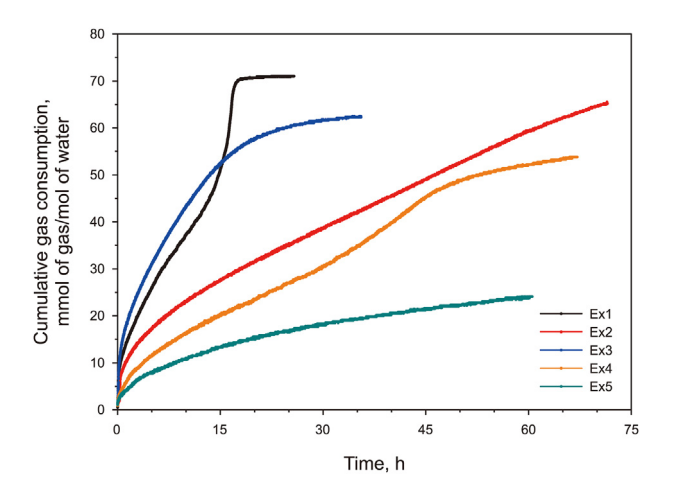
#### 3.1. Methane hydrate formation

#### 3.1.1. Effect of clay minerals on methane hydrate growth kinetics

In the experiments of MH formation, methane gas consumption for MH synthesis makes the pressure decrease. The thermal spike of the temperature during MH formation indicates that MH started to form and grow rapidly. MH formation in the sediments with different compositions shows different evolution of pressure and temperature with time as shown in Fig. 4. In Ex1 with pure quartz sediments, pressure and temperature reached the stabilization in a shortest duration of MH formation, while in Experiments 2–5 the duration of MH formation is longer in the sediments with clay mineral addition.

The cumulative consumption of methane gas during MH formation is shown in Fig. 5. The profiles of MH formation rate with formation time increase are seen in Fig. 6 and the detail of the formation experiments is in Table 3. The growth process of MH in different sediments can be divided as several stages based on the change of hydrate formation rate with time. MH formation in quartz sands in Ex1 displays multiple growth stages with two peaks of formation rate, including the first rapid growth stage, the slower formation stage, the second rapid growth stage and the final stable stage. The fastest rate of MH formation in the first rapid growth stage (20.2 mmol of gas/(mol of water · h)) is higher than that in the second rapid growth stage (11.8 mmol of gas/(mol of water · h)). The average MH formation rate is 2.8 mmol of gas/(mol of water·h). The multiple growth stages in Ex1 might be the result of the consumption and movement of water and methane gas which leads to the sufficient contact of water and gas during MH formation process.

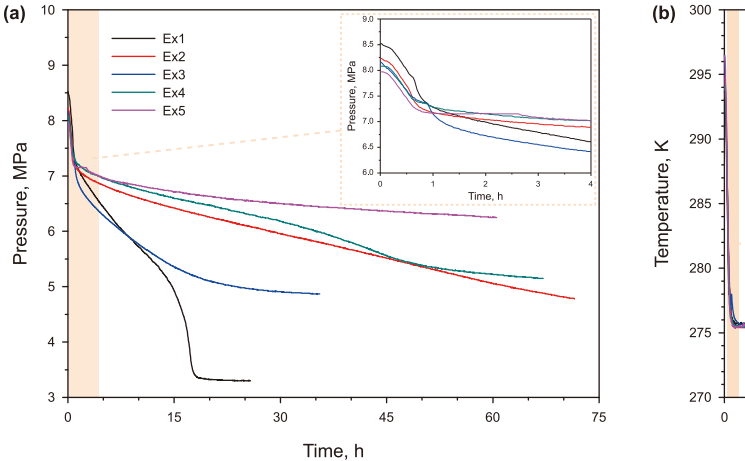
When mixing quartz sand with up to 20 wt% montmorillonite mineral, one common characteristic is that the MH growth rate decreases comparing with the case for pure quartz sands. MH formation process in montmorillonite-containing sediments does not show multiple rapid growth stages. In Ex2 with 10 wt% montmorillonite addition, MH formation process could be divided into two stages, including a rapid growth stage and a slow growth stage. The growth of MH in Ex3 admixed 20 wt% montmorillonite shows three different stages, including a rapid growth stage, a stage gradually decreasing in growth rate and a stable slow growth stage. The



**Fig. 5.** Cumulative consumption of methane gas with time in methane hydrate formation experiments.

addition of montmorillonite with 10 wt% (Ex2) and 20 wt% (Ex3) retard the MH formation rate in different degree. As shows in Table 3, the average formation rate both in stage 1 and in the whole process in Ex3 are higher than that in Ex2. Although the fastest rate and the average rate in stage 1 in Ex3 (23.1 and 5.4 mmol of gas/ (mol of water·h), respectively) are higher than that in Ex1, the average rate of the whole MH formation process in Ex3 (1.8 mmol of gas/(mol of water·h)) is lower than that in Ex1. The addition of montmorillonite inhibits the MH formation kinetics and the effect of inhibition is in difference with the variation of montmorillonite mass ratio.

Similar to montmorillonite, adding up to 20 wt% illite to quartz sand also decreases the MH formation rate comparing with the case of pure quartz sands. With the addition of illite, the stages of hydrate growth in the sediments show the different characteristics. In Ex4 with 10 wt% illite admixtures, the growth process consists of three stages. MH grows fastest in stage 1 and slower in stage 2 and 3, in which the formation rate in stage 3 is lower than that in stage 2. In the Ex5 with 20 wt% illite addition, MH growth can be divided into two stages, which is similar with Ex2. The addition of illite makes MH grow slow, and the maximum formation rate of MH decreases obviously with the increase of illite content in sediments. During the whole formation process, the average rate in Ex4 is 0.8 mmol of gas/(mol of water·h), higher than that in Ex5 with the



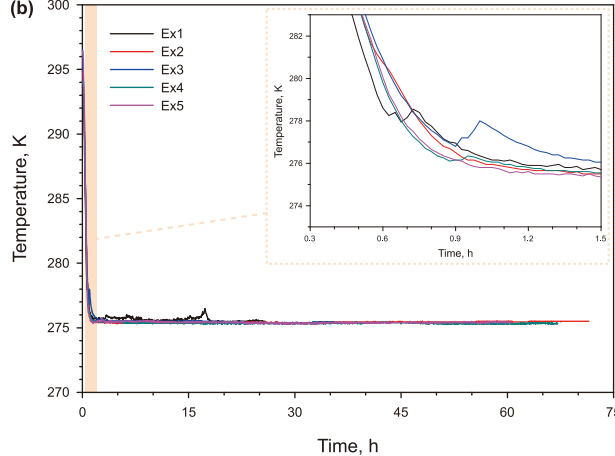
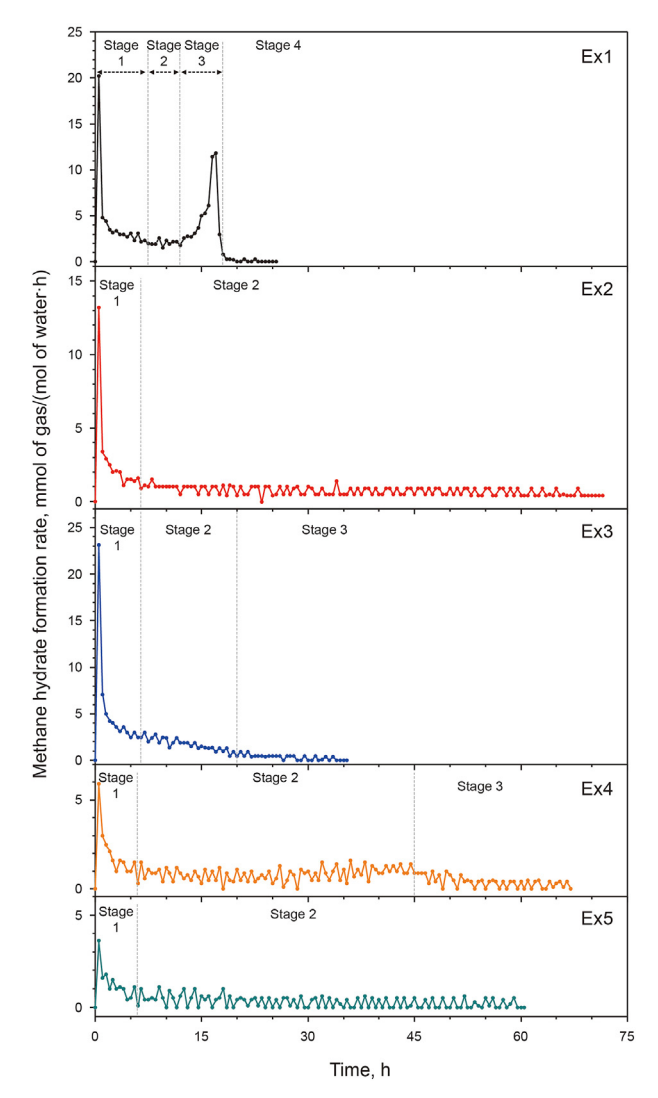


Fig. 4. Profiles of pressure and temperature in methane hydrate formation experiments.



**Fig. 6.** Profiles of methane hydrate formation rate in sediments with different components.

value of 0.4 mmol of gas/(mol of water  $\cdot$  h) (Table 3). Illite shows the obvious inhibition on MH formation kinetics and the inhibition effect is stronger with the increase of illite mass ratio.

In the montmorillonite-containing sediments, the formation rate of MH in Ex3 with 20 wt% montmorillonite is higher than that in Ex2 with 10 wt% montmorillonite (Fig. 6 and Table 3). It might be the result of the swelling nature and water adsorption of montmorillonite. The interlayer Na<sup>+</sup> of montmorillonite could lead water entering the interlayers of montmorillonite and make montmorillonite swell (e.g. Mitchell and Soga, 2005). Higher content of montmorillonite admixed in quartz sand leads to more water

content adsorbed into the interlayers of montmorillonite. It could result in the high porosity of the sediments (Liu et al., 2023), allow methane gas to fully contact with less available water and then facilitate the rate of MH formation. Therefore, the swelling nature of montmorillonite might have a significant effect on MH formation kinetics.

Due to the strong water absorption and swelling properties, the role of montmorillonite on MH formation is still inconsistent. For the MH formation in montmorillonite suspensions, MH forms at the interface of gas and water and the formation rate decreases with montmorillonite increase, which results from the denser suspension that would prevent mass transfer and retard MH growth (Nair et al., 2018; Ren et al., 2022). However, MH formation in clay-sand mixtures is more complex, Kumar et al. (2015) and Zhang et al. (2017) reported that as the mass ratio of montmorillonite increases, the rate of MH formation decreases, attributing to the swelling of montmorillonite leading to the porosity reduction. In this study, the addition of montmorillonite in quartz sands retards the MH formation rate but the rate decreases less with montmorillonite increase. This inconsistency might be due to the different sample preparation before MH formation. Kumar et al. (2015) presaturated the sediments with water before experiments, and Zhang et al. (2017) packed the sediments in the reactor and injected water before experiments. When montmorillonite contacts with water in the confined reactor, the swelling properties of montmorillonite play a negative role on the porosity (Aksu et al., 2015). In this study, water was mixed with the sediments before packing them in the reactor. The prewetting method of sample preparation would make water distribution more homogeneous and lead to a higher porosity due to the swelling of montmorillonite (Liu et al., 2023). In addition, the physicochemical property of montmorillonite used in different studies might be diverse due to various origins and treatment, and makes the results different.

In the illite-containing sediments, the maximum formation rate in Ex4 with 10 wt% illite is faster than that in Ex5 with 20 wt% illite content. It is consistent with the results of Chen et al. (2024) that the formation rate of MH decreases with the increasement of illite content at higher illite content in sandy sediments. The fine-sized and non-swelling illite particles would fill in the intergranular pore between quartz sands and reduce the pore spaces. It would prevent gas migration to the front of MH formation and result in decreasing in the formation rate of MH (Constant Agnissan et al., 2024). In our study, when illite and montmorillonite respectively mix with quartz sand with the same amount, the MH formation rate in montmorillonite-containing sediments is always higher than that in illite-containing sediments. Compared with montmorillonite, illite presents a stronger inhibition on the formation kinetics of MH. While Constant Agnissan et al. (2024) found that montmorillonite has a stronger inhibition on MH in comparison with illite. The difference between their results and this study in MH formation rate is likely attribute to the different sample preparation. In the study of Constant Agnissan et al. (2024), the dry claysand mixture sediments were packed into the vessel, followed by

**Table 3**Experiment results of methane hydrate formation in different sediments.

Exp. No.	Duration of MH formation, h	Methane gas consumption, mol	Average MH formation rate in Stage 1, mmol of gas/(mol of water·h)	Average MH formation rate in the whole process, mmol of gas/(mol of water·h)	Total methane gas consumption, mmol of gas/mol of water	Final water conversion, %
Ex1	25.75	0.350	4.6	2.8	71.0	42.6
Ex2	71.53	0.287	2.9	0.9	65.2	39.1
Ex3	35.56	0.268	5.4	1.8	62.3	37.4
Ex4	67.10	0.232	2.1	0.8	53.8	32.3
Ex5	60.52	0.104	1.4	0.4	24.1	14.4

water injection. As mentioned above, montmorillonite would reduce pore space in sediments under this sample preparation method. The physicochemical properties of clay minerals might also be various in different research.

## 3.1.2. Effect of clay minerals on gas consumption and water conversion

The final methane gas uptake and the water-to-hydrate conversion in MH formation experiments are summarized in Table 3 and presented in Figs. 5 and 7. The addition of clay minerals in sediments makes final gas consumption and water conversion decrease in this study. MH formation in the pure quartz in Ex1 consumes the highest amount of methane gas (71.0 mmol of gas/ mol of water) and the water conversion is the highest (42.6%). As the mass ratio of montmorillonite in quartz sediments increases from 10 to 20 wt%, the final gas consumption reduces from 65.2 mmol of gas/mol of water to 62.3 mmol gas/mol water. The water conversion in Ex2 is 39.1%, higher than that in Ex3 which is 37.4%. The MH formation in the illite-containing sediments shows the similar characteristics. In the guartz sediments with 10 wt% illite, the final uptake of methane gas is 53.8 mmol gas/mol water and the water conversion is 32.3%. While in the quartz sands admixed with 20 wt% illite, the final gas uptake is 24.1 mmol gas/ mol water and the water conversion is 14.4%.

The increase of montmorillonite or illite in quartz-dominant sediments reduces the final gas consumption and water conversion in MH formation experiments. It might be due to the surface property of the two clay minerals which is negatively charged and adsorbs bound water (Sun et al., 2021). Higher content of clay minerals in sediments would lead to the larger amount of bound water adsorbed on clay mineral surface, which does not participate in MH formation, depress water activity (Clennell et al., 1999; Wang et al., 2023) and thus reduce the water-to-hydrate conversion. The result of our study is consistent with the report of Kumar et al. (2015) and Zhang et al. (2017) that with the mass ratio of montmorillonite increase, the water conversion and total gas consumption decrease. In our study, the reduction of methane gas and water uptake in illite-containing sediments is larger than that in montmorillonite-containing sediments. It might be caused by the difference in electronegativity of the two clay minerals that illite has a larger electronegativity unit cell in comparison with montmorillonite (Mi et al., 2022; Mitchell and Soga, 2005). Larger

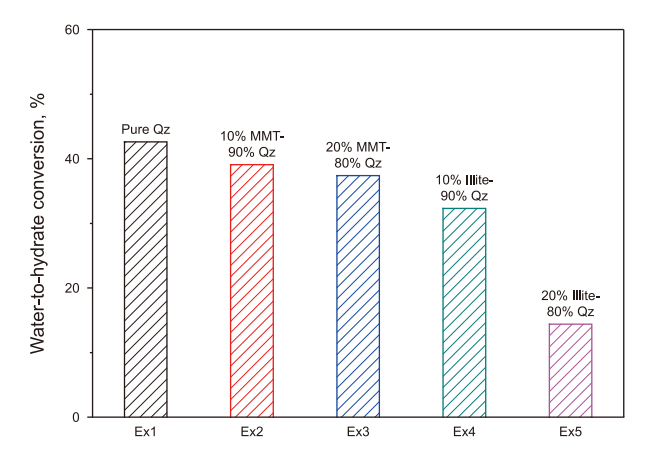


**Fig. 7.** Water-to-hydrate conversion in methane hydrate formation experiments with different sediments. Qz: Quartz, MMT: Montmorillonite.

electronegativity of clay minerals would bind more water molecules to form an interfacial water layer on the surface, decrease water activity, repel methane molecules, and strongly inhibit MH formation (Li et al., 2020; Mi et al., 2022, 2023). Therefore, illite shows the stronger inhibition on final gas uptake and water-to-hydrate conversion than montmorillonite during MH formation process.

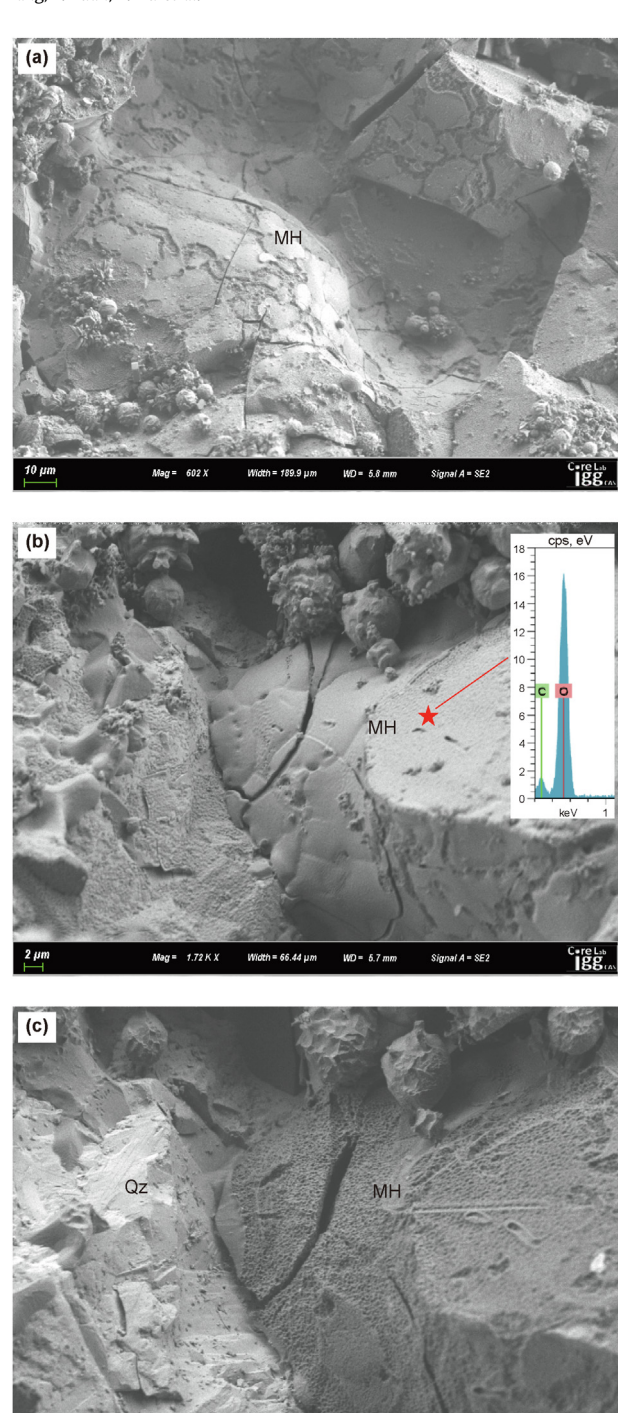
#### 3.2. Cryo-SEM observation of sand sediments

In the pure quartz sands, quartz particles are not easy to been identified in this study but methane hydrate could be widely observed as shown in Fig. 8. The widespread distribution of methane hydrate with smooth surface is seen in the local area in Fig. 8(a). Moreover, methane hydrate, identified by EDS analysis with carbon peak, distributes in the pore within quartz sands in Fig. 8(b). The same area was scanned again after 10 min as shown in Fig. 8(c). The surface of the hydrate particle at the middle and right in Fig. 8(b) became porous in Fig. 8(c). Due to the electron beam scanning for local-area observation and EDS analysis (Stern and Lorenson, 2014), MH dissociates below the ice point with the production of methane gas and ice, and make MH porous. And the brighter quartz particle at the left in Fig. 8(c) was appeared after the sublimation of the outer coating methane hydrate at the left in Fig. 8(b).

To understand the effects of montmorillonite and illte on MH formation in microscale and nanoscale, the microstructure of the sediments in Experiments 3 and 5 were also observed (Figs. 9 and 10). Fig. 9(a) and (b) indicate that the undulating aggregates of montmorillonite do not widely coat on the surface of quartz grain. Montmorillonite particles typically accumulate as aggregates and the individual particles are hardly to be identified. Porous materials are widely distributed in the sediments in Ex3 in Fig. 9(a) and (b). EDS analyzed the material phase along the yellow arrow in Fig. 9(b) and the analysis results is shown in Fig. 9(c). Porous material is the dissociating MH identified with high amount of carbon element. The dense material is the ice with abundant oxygen element. Montmorillonite aggregate is identified with the high amount of sodium element. Due to the depressurization and the damage from electron beam scanning, the surface of the MH dissociated below the ice point is porous. Combined with the morphology and EDS analysis in Fig. 9, the edges of montmorillonite aggregate directly contact with the surrounding dense water ice which separates methane hydrate from the montmorillonite aggregate.

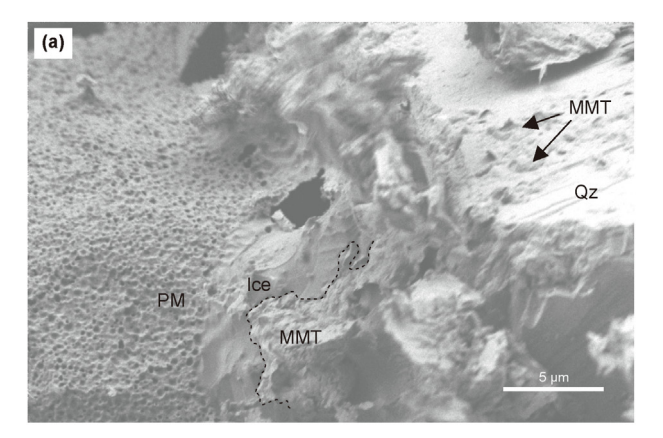
While the arrangement of illite particles is different from that of montmorillonite in clay-containing quartz sands. Fig. 10 indicates that illite particles in Ex5 assemble tightly as surface-overlapped stacks. Less water is trapped within illite aggregates. Regardless of the presence of quartz particle in the local area, illite platelets tightly contact with pore water ice as showing in Fig. 10. No widespread distribution of methane hydrate was observed in illite-containing quartz sands in this investigation.

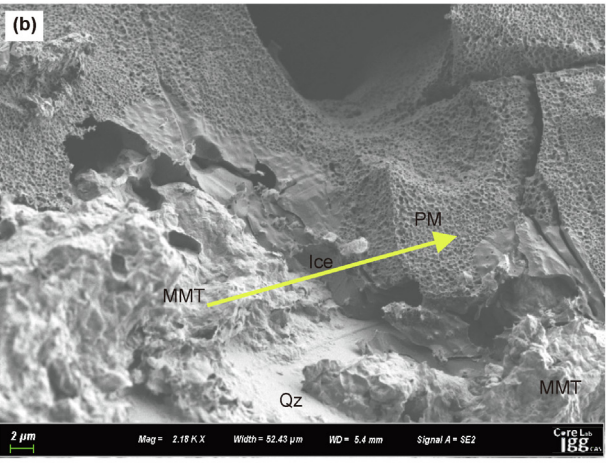
Montmorillonite and illite show different particle arrangements in sand sediments due to their different physicochemical properties. Montmorillonite aggregates distribute as several clay clusters in sand sediments, which might be the results of swelling properties and water adsorption in the interlayers through the interlayer Na<sup>+</sup> cation. While illite typically has higher surface charge density due to the interlayer K<sup>+</sup> cation, illite platelets show the stronger interlayer energy and tightly stack together (Jia et al., 2023; Zhu et al., 2022). The face-to-face particle packing in preferred orientation would make sediments have low porosity (Bennett, 1981). Moreover,



**Fig. 8.** Microstructure of the pure quartz sediments. **(a)** The widespread distribution of methane hydrate. **(b)** Methane hydrate particle filling in the pore. **(c)** The same area of (b) after 10-min observation. MH: Methane hydrate, Qz: Quartz.

different from montmorillonite aggregates, the large area of illite aggregates coating on water ice in Fig. 10(b) would prevent the contact of free gas and water and thus significantly retard MH formation rate. Therefore, due to the differences in the physicochemical properties, montmorillonite and illite have different effects on pore spaces and the gas-water contact, and lead to the dramatic difference in MH formation rate between the Ex3 and Ex5.





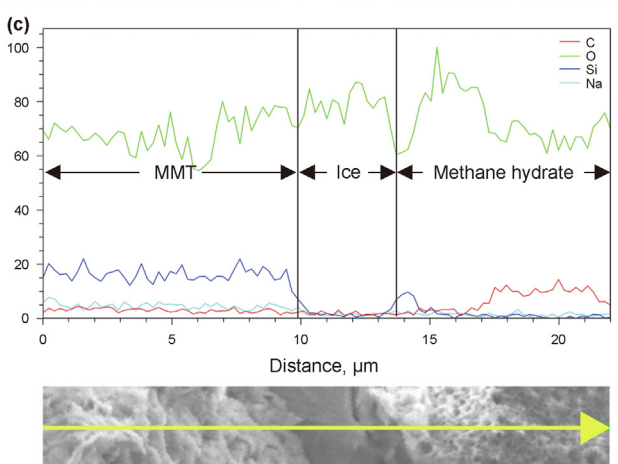


**Fig. 9.** Microstructure of the sediments recovered in Ex3. PM: Porous material, MMT: Montmorillonite and Qz: Quartz.

#### 3.3. Methane hydrate dissociation

## 3.3.1. Evolution of pressure and temperature during depressurization

During depressurization process, the pressure and temperature evolution in the three dissociation experiments appears the similar characteristics (Fig. 11). The pressure reduction could be divided into 3 stages. The pressure declines linearly in the stage 1 due to the constant release of free methane gas before reaching the near-equilibrium pressure. The reduction of pressure becomes slow

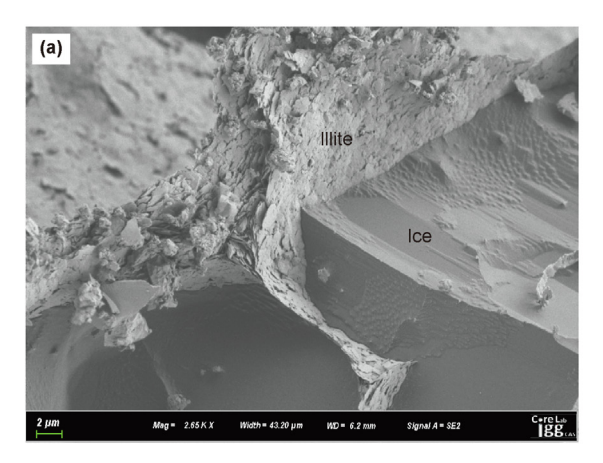




Fig. 10. Illite aggregates in the sediments recovered in Ex5.

when MH begins to decompose in the stage 2. After MH dissociation, the pressure decreases faster in the stage 3 due to the release of free methane gas. The MH dissociation is endothermic and the temperature decreases during MH decomposition in stage 2. In stage 3 the temperature gradually increases to the experimental temperature around 275.5 K by the heat supplement from the surroundings. The reduction of temperature during MH dissociation is different in the three MH dissociation experiments. The temperature decrease during MH dissociation in Ex6 is steady and the lowest temperature is 275.1 K. During MH decomposing, the lowest temperature in Ex7 in montmorillonite-containing sediments is 274.8 K and that in Ex8 with illite addition is 274.9 K. Temperature reduction in clay-containing sediments in Experiments 7 and 8 is more dramatic compared with that in pure quartz in Ex6.

#### 3.3.2. Dissociation kinetics of methane hydrate

During the depressurization process, the pressure dropped slowly due to the low constant rate of gas release and no water was produced. When the pressure declines to the near-equilibrium pressure (3.29 MPa) at 275.2 K, MH stored in sediments gradually decomposes. Detail results of MH dissociation experiments are presented in Table 4 and Fig. 12. The amount of methane gas released from MH dissociation in Experiments 6—8 is 0.399, 0.303 and 0.147 mol, respectively. The amount of MH storage and the gas recovered from MH in pure quartz sediments is higher than that in the sediments mixed with clay minerals (Fig. 12(a)). Methane gas released from MH dissociation in illite-containing sediments is less than that in sediments containing montmorillonite.

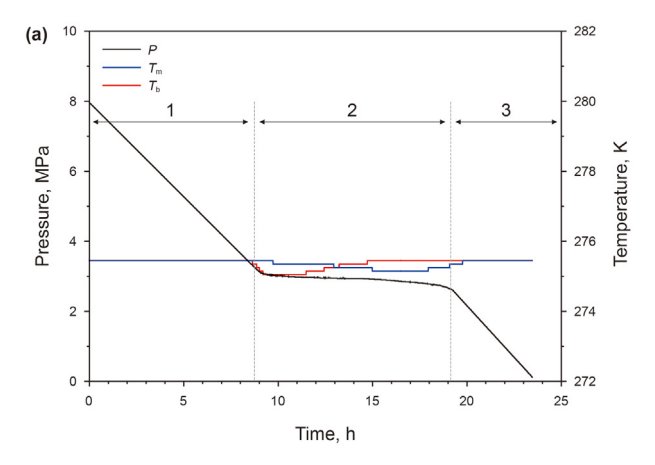
MH decomposes faster in the clay-containing sediments than that in pure quartz. The average gas production rate during MH dissociation is 15.5, 19.1 and 35.9 m³ gas/(m³ hydrate·h) in Experiments 6–8, respectively (Table 4). The average dissociation rate in illite-containing sediments is the highest, the rate in montmorillonite-containing sediments is higher than that in pure quartz sediments. Fig. 12(b) indicates that during MH dissociation, the maximum gas production rate in illite-containing sediments is much faster than the other two dissociation experiments. In comparison with quartz, montmorillonite and illite would facilitate MH dissociation. It might be due to the effect of the cations on the surface of clay minerals which can accelerate the processes of MH dissociation (Fang et al., 2022; Waldron and English, 2018). The promotion effect of K+ on MH dissociation is greater than that of Na+ (Chen et al., 2023). Consequently, illite shows a stronger

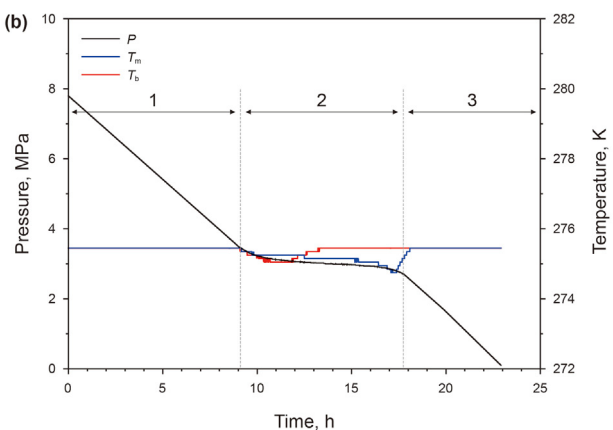
promotion than montmorillonite on MH dissociation kinetics.

In addition, the distributions of MH in the sediments with/ without clay minerals might also influence the dissociation rate of MH. In this study, the widespread distribution of MH was observed both in pure quartz sediments (Fig. 8(a)) and in montmorillonitecontaining sediments (Fig. 9(b)). However, the MH coating on the outer surface of minerals and the massive MH particles as large in Fig. 8(b) were not observed in the clay-containing sediments in this study. MH has been investigated from molecular simulation insights that it dissociates from the outer surface to the center as the layer-by-layer in the pore composed of quartz or clay minerals (Bagherzadeh et al., 2013; Fang et al., 2022, 2024). Compared with the larger MH particles in pure quartz sediments, the thin and widespread distribution of MH or the small MH particles in claycontaining sediments might expose more outer surface of MH and decompose synchronously (Fig. 13). It would make the temperature reduction more dramatical in clay-containing sediments. Therefore, the dissociation rate of MH in the clay-containing sediments is more rapid in comparison with that in pure quartz sediments.

## 3.4. Implication for natural gas hydrate accumulation and production

Quartz, montmorillonite and illite are the dominant mineral compositions of marine GHBS such as in the East Nankai offshore, the South China Sea and the Blake Ridge (Collett and Wendlandt, 2000; Egawa et al., 2015; Wang et al., 2022). Although mineral composition affects MH formation kinetics, it would not significantly affect the accumulation of natural gas hydrate in hydrate reservoirs over the long geological time scale. But secondary MH formation might occur during natural gas hydrate production and cause large amount of MH blocking pores and throats to decrease the gas production (Wang et al., 2017). In addition, during the recovery of hydrate-bearing sediments, it might not be easy to keep MH stable in hydrate reservoirs with higher content of illite compared with the reservoirs dominantly composed of montmorillonite or quartz. Moreover, the dissociation degree of hydrate influences the mechanical properties of GHBS, and possibly causes submarine landslide, local strata deformation and infrastructure instability during gas hydrate production (Dhakal and Gupta, 2023; Lee et al., 2020; Song et al., 2019). Due to the difference in dissociation rate, the illite-rich GHBS might not have the same influence on submarine slope instability compared with the GHBS rich in





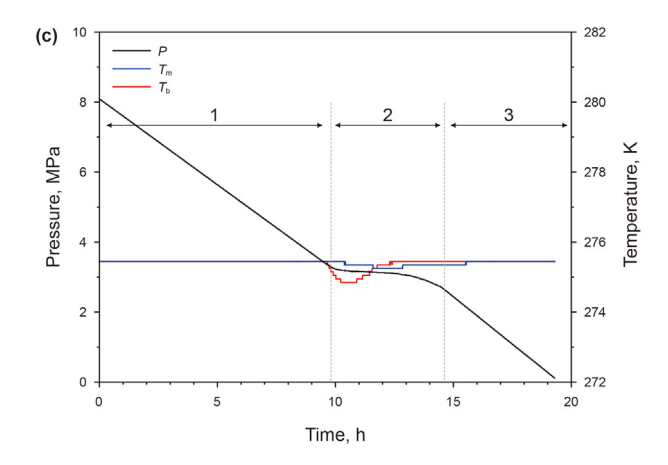


Fig. 11. Pressure and temperature evolution in methane hydrate dissociation experiments Ex6 (a), Ex7 (b) and Ex8 (c).

montmorillonite or quartz. Different safety strategies for gas production and sediment recovery should be developed based on the mineral compositions of hydrate-bearing sediments. Therefore, the effects of clay minerals on MH formation and dissociation would provide deep insights into geological investigations of gas hydrate reservoirs and natural gas production.

#### 4. Conclusions

In this study, the effects of clay minerals on MH formation and dissociation were investigated through mixing montmorillonite and illite separately with quartz sands to synthesize and decompose MH. Microstructure of the sediments mixed with/without the two clay minerals were observed by cryo-SEM. The results are summarized as follows.

- (1) Montmorillonite and illite both show an inhibition effect on MH formation kinetics and water-to-hydrate conversion when comparing with pure quartz sands. Illite has a stronger inhibition on MH in comparison of montmorillonite. The lower mass ratio (10 wt%) of montmorillonite significantly retards MH formation rate, and the higher mass ratio (20 wt%) has the less retardation on the rate. The increase of illite mass ratio (0–20 wt%) in the mixture sediments presents the strong inhibition on MH formation rate. The presence of montmorillonite and illite in quartz sands could both reduce the water-to-hydrate conversion. As the mass content of clay minerals increases, the water-to-hydrate conversion gradually decreases.
- (2) In the clay-containing sands, montmorillonite particles aggregate separately as several clusters while illite particles pack as face-to-face configuration under the interaction with water. The structure of illite aggregates would reduce pore space, prevent the contact of methane gas and water, and lead to the stronger inhibition on MH formation kinetics.
- (3) Under the depressurization with constant gas release rate, both montmorillonite and illite show a promotion on MH dissociation kinetics in comparison with quartz. Temperature drops more dramatically in clay-containing sediments during MH dissociation. Physicochemical properties of clay minerals and MH distribution in clay-containing sediments lead to the faster dissociation rate of MH in comparison with the rate in pure quartz sediments.

The different effects of montmorillonite and illite on the kinetics of MH formation and dissociation in our study would provide some insights on preventing secondary MH formation and designing safety strategies during gas hydrate production in clay-rich hydrate reservoirs. Further studies could focus on using artificial intelligence to integrate multi-scale studies for understanding the

 Table 4

 Experiment results of methane hydrate dissociation in different sediments.

Exp. Experiment No. duration, h	Initial methane gas hydrate, mol	Gas recovered from hydrate dissociation, mol	Average gas production rate from hydrate dissociation, $m^3$ gas/( $m^3$ hydrate $\cdot$ h)
Ex6 23.5	0.402	0.399	15.5
Ex7 22.9 Ex8 19.3	0.313 0.148	0.303 0.147	19.1 35.9

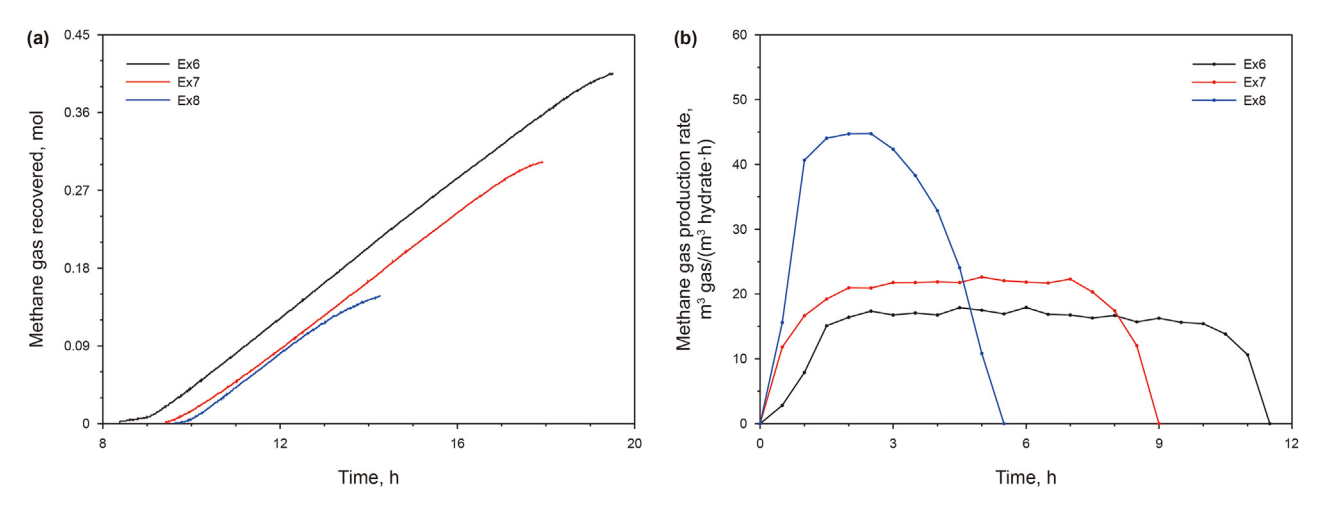


Fig. 12. Methane gas production during methane hydrate dissociation. (a) The amount of methane gas released from hydrate dissociation. (b) Normalized methane gas production rate.

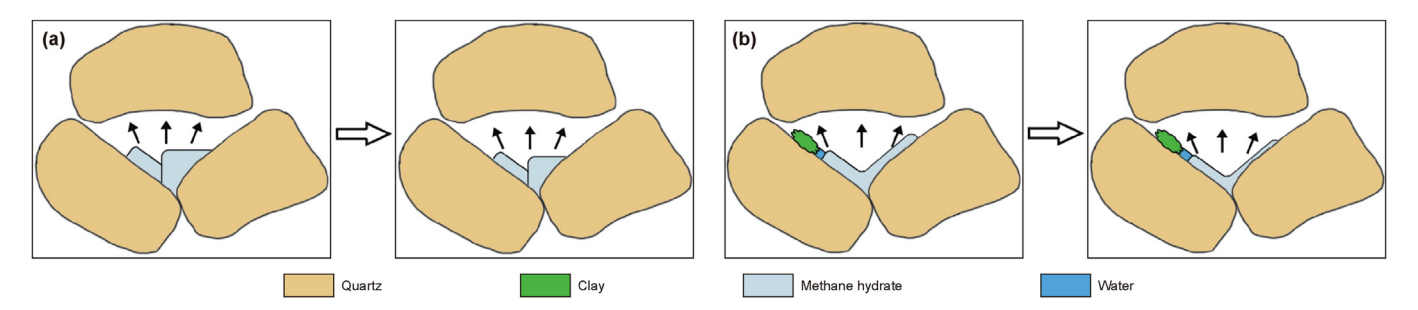


Fig. 13. Schematic diagram of MH dissociation in (a) pure quartz sediments and (b) clay-containing sediments.

accumulation of gas hydrate and predicting gas hydrate exploration and production.

#### **CRediT authorship contribution statement**

**Xinxu Wang:** Writing — review & editing, Writing — original draft, Methodology, Investigation, Conceptualization. **Yuan Yuan:** Methodology. **Zhongming Du:** Methodology. **Bo Liu:** Writing — review & editing. **Chenlu Xu:** Writing — review & editing. **Jijin Yang:** Writing — review & editing, Supervision, Project administration, Methodology, Investigation, Funding acquisition.

#### Declaration of interests

The authors declare that they have no known competing financial interests or personal relationships that could have appeared to influence the work reported in this paper.

#### Acknowledgments

This research was supported by the Key Research Program of the Institute of Geology & Geophysics, CAS (Grant No. IGGCAS-201903).

#### References

Aksu, I., Bazilevskaya, E., Karpyn, Z.T., 2015. Swelling of clay minerals in unconsolidated porous media and its impact on permeability. GeoResJ 7, 1–13. https://doi.org/10.1016/j.grj.2015.02.003.

Bagherzadeh, S.A., Alavia, S., Ripmeester, J.A., et al., 2013. Evolution of methane during gas hydrate dissociation. Fluid Phase Equilib. 358, 114–120. https:// doi.org/10.1016/j.fluid.2013.08.017.

Bennett, R.H., 1981. Clay fabric of selected submarine sediments: fundamental

properties and models. J. Sediment. Petrol. 51, 217–232. https://doi.org/10.1306/212F7C52-2B24-11D7-8648000102C1865D.

Boswell, R., Collett, T.S., 2006. The gas hydrates resource pyramid. Fire in the Ice 3, 5–7.

Boswell, R., Collett, T.S., 2011. Current perspectives on gas hydrate resources. Energy Environ. Sci. 4 (4), 1206–1215. https://doi.org/10.1039/C0EE00203H.

Canals, M., Lastras, G., Urgeles, R., et al., 2004. Slope failure dynamics and impacts from seafloor and shallow sub-seafloor geophysical data: case studies from the costa project. Mar. Geol. 213 (1–4), 9–72. https://doi.org/10.1016/j.margeo.2004.10.001.

Cha, S.B., Ouar, H., Wildeman, T.R., et al., 1988. A third-surface effect on hydrate formation. J. Phys. Chem. 92, 6492–6494. https://doi.org/10.1021/j100334a006. Chen, B., Li, K., Sun, H., et al., 2023. Promoting effect of common marine cations on

Lhen, B., Li, K., Sun, H., et al., 2023. Promoting effect of common marine cations on hydrate dissociation and structural evolution under a static electric field. J. Phys. Chem. B. 127, 698-709. https://doi.org/10.1021/acs.jpcb.2c05382.

Chen, C., Zhang, Y., Li, X., et al., 2024. Investigations into methane hydrate formation, accumulation, and distribution in sediments with different contents of illite clay. Appl. Energy. 359, 122661. https://doi.org/10.1016/j.apenergy.2024.122661.

Chong, Z.R., Pujar, G.A., Yang, M., et al., 2016. Methane hydrate formation in excess water simulating marine locations and the impact of thermal stimulation on energy recovery. Appl. Energy. 177, 409–421. https://doi.org/10.1016/j.ianenergy.2016.05.077

Chong, Z.R., Koh, J.W., Linga, P., 2017. Effect of KCl and MgCl<sub>2</sub> on the kinetics of methane hydrate formation and dissociation in sandy sediments. Energy 137, 518–529. https://doi.org/10.1016/j.energy.2017.01.154.

Clennell, M.B., Hovland, M., Booth, J.S., et al., 1999. Formation of natural gas hydrates in marine sediments 1. Conceptual model of gas hydrate growth conditioned by host sediment properties. J. Geophys. Res. 104 (B10), 22985–23003. https://doi.org/10.1029/1999JB900175.

Collett, T.S., Wendlandt, R.F., 2000. Formation evaluation of gas hydrate-bearing marine sediments on the Blake Ridge with downhole geochemical log measurements. Proc. Ocean Drill. Progr. Sci. Results 164, 199–215.

Constant Agnissan, A.C., Guimpier, C., Terzariol, M., et al., 2024. Influence of clay-containing sediments on methane hydrate formation: impacts on kinetic behavior and gas storage capacity. J. Geophys. Res. Solid Earth. 128, e2023JB027333. https://doi.org/10.1029/2023JB027333.

Cygan, R.T., Guggenheim, S., Koster van Groos, A.F., 2004. Molecular models for the intercalation of methane hydrate complexes in montmorillonite clay. J. Phys.

- Chem. B 108, 15141-15149. https://doi.org/10.1021/JP037900X.
- Dhakal, S., Gupta, I., 2023. Slope instability of submarine sediments due to hydrate dissociation: a case study of Northern Cascadia Margin. Geoenergy. sci. eng. 223, 211558. https://doi.org/10.1016/j.geoen.2023.211558.
- Egawa, K., Nishimura, O., Izumi, S., et al., 2015. Bulk sediment mineralogy of gas hydrate reservoir at the East Nankai offshore production test site. Mar. Petrol. Geol. 66, 379–387. https://doi.org/10.1016/j.marpetgeo.2015.02.039.
- Fang, B., Lü, T., Ning, F., et al., 2022. Facilitating gas hydrate dissociation kinetics and gas migration in clay interlayer by surface cations shielding effects. Fuel 318, 123576. https://doi.org/10.1016/ji.fuel.2022.123576.
- Fang, B., Lü, T., Li, W., et al., 2024. Microscopic insights into poly- and monocrystalline methane hydrate dissociation in Na-montmorillonite pores at static and dynamic fluid conditions. Energy 288, 129755. https://doi.org/10.1016/j.energy.2023.129755.
- Feng, Y., Qu, A., Han, Y., et al., 2023. Effect of gas hydrate formation and dissociation on porous media structure with clay particles. Appl. Energy. 349, 121694. https://doi.org/10.1016/j.apenergy.2023.121694.
- Guo, G., Zhang, Z., 2021. Open questions on methane hydrate nucleation. Commun. Chem. 4, 102. https://doi.org/10.1038/s42004-021-00539-6.
- Jia, J., Wu, D., Lin, J., et al., 2023. Molecular dynamics simulation of illite: from particle associations to hydration properties. Appl. Clay Sci. 234, 106850. https://doi.org/10.1016/j.clay.2023.106850.
- Kumar, A., Sakpal, T., Roy, S., et al., 2015. Methane hydrate formation in a test sediment of sand and clay at various levels of water saturation. Can. J. Chem. 93, 874—881. https://doi.org/10.1139/cjc-2014-0537.
- Kvenvolden, K.A., 2002. Methane hydrate in the global organic carbon cycle. Terra Nova 14, 302–306. https://doi.org/10.1046/j.1365-3121.2002.00414.x.
- Lee, Y., Deusner, C., Kossel, E., et al., 2020. Influence of CH<sub>4</sub> hydrate exploitation using depressurization and replacement methods on mechanical strength of hydrate-bearing sediment. Appl. Energy. 277, 115569. https://doi.org/10.1016/ j.apenergy.2020.115569.
- Li, J., Ye, J., Qin, X., et al., 2018. The first offshore natural gas hydrate production test in South China Sea. China Geology 1, 5–16. https://doi.org/10.31035/cg2018003.
- Li, J., Lu, J., Kang, D., et al., 2019. Lithological characteristics and hydrocarbon gas sources of gas hydrate-bearing sediments in the Shenhu area, South China Sea: Implications from the W01B and W02B sites. Mar. Geol. 408, 36–47. https://doi.org/10.1016/j.margeo.2018.10.013.
- Li, Y., Chen, M., Liu, C., et al., 2020. Effects of layer-charge distribution of 2:1 clay minerals on methane hydrate formation: a molecular dynamics simulation study. Langmuir 36, 3323–3335. https://doi.org/10.1021/acs.langmuir.0c00183.
- Liu, Z., Zheng, J., Wang, Z., et al., 2023. Effect of clay on methane hydrate formation and dissociation in sediment: Implications for energy recovery from clayeysandy hydrate reservoir. Appl. Energy 341, 121064. https://doi.org/10.1016/ j.apenergy.2023.121064.
- Ma, X., Jiang, D., Lu, J., et al., 2022. Hydrate formation and dissociation characteristics in clayey silt sediment. J. Nat. Gas Sci. Eng. 100, 104475. https://doi.org/10.1016/j.jngse.2022.104475.
- Meazell, P.K., Flemings, P.B., Santra, M., et al., 2020. Sedimentology and stratigraphy of a deep-water gas hydrate reservoir in the northern Gulf of Mexico. AAPG (Am. Assoc. Pet. Geol.) Bull. 104 (9), 1945–1969. https://doi.org/10.1306/ 05212019027.
- Mi, F., He, Z., Zhao, Y., et al., 2022. Effects of surface property of mixed clays on methane hydrate formation in nanopores: a molecular dynamics study. J. Colloid Interface Sci. 627, 681–691. https://doi.org/10.1016/ji.jcis.2022.07.101.
- Mi, F., He, Z., Cheng, L., et al., 2023. Molecular dynamics simulation on methane hydrate formation in clay nanopores of edge surfaces. Appl. Clay Sci. 243, 107069. https://doi.org/10.1016/j.clay.2023.107069.
- Mitchell, J.K., Soga, K., 2005. Fundamentals of Soil Behavior, third ed. John Wiley & Sons, USA, New York.
- Moridis, G.J., Kim, J., Reagan, M.T., et al., 2013. Feasibility of gas production from a gas hydrate accumulation at the UBGH2-6 site of the Ulleung basin in the Korean East Sea. J. Petrol. Sci. Eng. 108, 180–210. https://doi.org/10.1016/ j.petrol.2013.03.002.
- Nair, V.C., Prasad, S.K., Kumar, R., et al., 2018. Energy recovery from simulated clayey gas hydrate reservoir using depressurization by constant rate gas release, thermal stimulation and their combinations. Appl. Energy. 225, 755–768. https://doi.org/10.1016/j.apenergy.2018.05.028.
- Park, S.H., Sposito, G., 2003. Do montmorillonite surfaces promote methane hydrate formation? Monte Carlo and molecular dynamics simulations. J. Phys. Chem. B. 107, 2281–2290. https://doi.org/10.1021/jp021427q.
- Phillips, S.C., Johnson, J.E., Underwood, M.B., et al., 2014. Long-timescale variation in bulk and clay mineral composition of Indian continental margin sediments in

- the Bay of Bengal, Arabian Sea, and Andaman Sea. Mar. Petrol. Geol. 58, 117–138. https://doi.org/10.1016/j.marpetgeo.2014.06.018.
- Piñero, E., Marquardt, M., Hensen, C., et al., 2013. Estimation of the global inventory of methane hydrates in marine sediments using transfer functions. Biogeosciences 10, 959–975. https://doi.org/10.5194/bg-10-959-2013.
- Poling, B.E., Prausnitz, J.M., O'connell, J.P., 2001. The Properties of Gases and Liquids, fifth ed. Mcgraw-hill, New York.
- Ren, J., Liu, X., Niu, M., et al., 2022. Effect of sodium montmorillonite clay on the kinetics of CH<sub>4</sub> hydrate - implication for energy recovery. Chem. Eng. J. 437, 135368. https://doi.org/10.1016/j.cej.2022.135368.
- Ren, J., Zeng, S., Chen, D., et al., 2023. Roles of montmorillonite clay on the kinetics and morphology of CO<sub>2</sub> hydrate in hydrate-based CO<sub>2</sub> sequestration. Appl. Energy. 340, 120997. https://doi.org/10.1016/j.apenergy.2023.120997.
- Ren, J., Yin, Z., Lu, H., et al., 2024. Effects of South China Sea clayey-silty sediments on the kinetics and morphology of CH<sub>4</sub> hydrate: implication on energy recovery. Appl. Energy. 367, 123399. https://doi.org/10.1016/j.apenergy.2024.123399.
- Ruppel, C., 2007. Tapping methane hydrates for unconventional natural gas. Elements 3, 193–199. https://doi.org/10.2113/gselements.3.3.193.
- Ruppel, C., 2015. Permafrost-associated gas hydrate: is it really approximately 1% of the global system? J. Chem. Eng. Data. 60 (2), 429–436. https://doi.org/10.1021/je500770m.
- Ruppel, C.D., Kessler, J.D., 2017. The interaction of climate change and methane hydrates. Rev. Geophys. 55, 126–168. https://doi.org/10.1002/2016RG000534.
- Shaibu, R., Sambo, C., Guo, B., et al., 2021. An assessment of methane gas production from natural gas hydrates: Challenges, technology and market outlook. Adv. Geo-Energy Res. 5 (3), 318–332. https://doi.org/10.46690/ager.2021.03.07.
- Sloan, E.D., Koh, C., 2007. Clathrate Hydrates of Natural Gases, third ed. CRC Press. Smith, J.M., Van Ness, H.C., Abbott, M.M., 2001. Introduction to Chemical Engineering Thermodynamics, sixth ed. McGraw-Hill, New York.
- Song, B., Cheng, Y., Yan, C., et al., 2019. Seafloor subsidence response and submarine slope stability evaluation in response to hydrate dissociation. J. Nat. Gas Sci. Eng. 65, 197–211. https://doi.org/10.1016/j.jngse.2019.02.009.
- Stern, L.A., Lorenson, T.D., 2014. Grain-scale imaging and compositional characterization of cryo-preserved India NGHP 01 gas-hydrate-bearing cores. Mar. Petrol. Geol. 58, 206–222. https://doi.org/10.1016/j.marpetgeo.2014.07.027.
- Sun, Y., Jiang, S., Li, S., et al., 2021. Hydrate formation from clay bound water for CO<sub>2</sub> storage. Chem. Eng. J. 406, 126872. https://doi.org/10.1016/j.cej.2020.126872.
- Waite, W.F., Santamarina, J.C., Cortes, D.D., et al., 2009. Physical properties of hydrate-bearing sediments. Rev. Geophys. 47, RG4003. https://doi.org/10.1029/ 2008RG000279.
- Waldron, C.J., English, N.J., 2018. System-density fluctuations and electro dissociation of methane clathrate hydrates in externally applied static electric fields. J. Chem. Therm. 117, 68–80. https://doi.org/10.1016/j.jct.2017.08.016.
- Wang, P., Yang, M., Chen, B., et al., 2017. Methane hydrate reformation in porous media with methane migration. Chem. Eng. Sci. 168, 344–351. https://doi.org/10.1016/j.ces.2017.04.036.
- Wang, R., Liao, B., Wang, J., et al., 2023. Microscopic molecular insights into methane hydrate growth on the surfaces of clay minerals: experiments and molecular dynamics simulations. Chem. Eng. J. 451, 138757. https://doi.org/ 10.1016/j.cej.2022.138757.
- Wang, X., Feng, J., Zhang, L., et al., 2022. Mineralogy and pore characteristics of marine gas hydrate-bearing sediments in the northern South China Sea. Mar. Petrol. Geol. 141, 105711. https://doi.org/10.1016/j.marpetgeo.2022.105711.
- Wang, X., Yuan, Y., Du, Z., et al., 2024. Mineral effects on methane hydrate formation and distribution in sand sediments. Geoenergy. sci. eng. 243, 213379. https:// doi.org/10.1016/j.geoen.2024.213379.
- Yang, S., Choi, J.C., Vanneste, M., et al., 2018. Effects of gas hydrates dissociation on clays and submarine slope stability. Bull. Eng. Geol. Environ. 77, 941–952. https://doi.org/10.1007/s10064-017-1088-2.
- Yin, Z., Chong, Z.R., Tan, H.K., et al., 2016. Review of gas hydrate dissociation kinetic models for energy recovery. J. Nat. Gas Sci. Eng. 35, 1362–1387. https://doi.org/ 10.1016/j.jngse.2016.04.050.
- Zeng, H., Zhang, Y., Zhang, L., et al., 2022. Effects of the NaCl concentration and montmorillonite content on formation kinetics of methane hydrate. J. Mar. Sci. Eng. 10 (4), 548. https://doi.org/10.3390/jmse10040548.
- Zhang, L., Xu, S., Li, X., et al., 2017. Reaction kinetic characteristics and model of methane hydrate formation in porous media. Energy & Fuels 31 (8), 8548–8559. https://doi.org/10.1021/acs.energyfuels.7b00958.
- Zhu, H., Whittle, A.J., Pellenq, R.J.M., 2022. Potential of mean force for face-face interactions between pairs of 2:1 clay mineral platelets. Langmuir 38 (43), 13065–13074. https://doi.org/10.1021/acs.langmuir.2c01632.